Central European Journal of Energetic Materials
ISSN 1733-7178; e-ISSN 2353-1843

Cent. Eur. J. Energ. Mater. 2023, *20*(1): 36-49; DOI 10.22211/cejem/162859
Article is available in PDF-format, in colour, at:
https://ipo.lukasiewicz.gov.pl/wydawnictwa/cejem-woluminy/vol-20-nr-1/

Research paper

Photo-thermal Decomposition of HNS Surface by 532 nm Laser Irradiation: Spectral and Quantitative Analysis using In-Situ XPS- Quadrupole MS Technique

Yi Sun[1,*)], **Tao Xu**[1,2)], **Min Shui**[3)]

[1)] *School of Materials Science and Engineering, Southwest University of Science and Technology, China*

[2)] *Institute of Chemical Materials, China Academy of Engineering Physics, Mianyang, Sichuan, China*

[3)] *Research Center of Laser Fusion, China Academy of Engineering Physics, Mianyang Sichuan, Mianyang, Sichuan, China*

* *E-mail:* hmily-sunny@163.com

Abstract: A novel approach for studying the photo-thermal decomposition of HNS (2,2',4,4',6,6'-hexanitrostilbene) at 532 nm induced by a 10-nanosecond (ns) laser pulse is described. In this method, in-situ X-ray photoelectron spectrometer (XPS) – laser-quadrupole mass spectrometer on-line equipment was designed. New peaks at binding energies of 399.7 eV in the N 1s XPS spectrum and 288.6 eV in the C 1s spectrum showed that nitro-nitrite isomerization with subsequent release of NO occurs in the laser-induced decomposition of HNS. A new peak at 30 m/z in the mass spectrum is also associated with the mechanism of the nitro-nitrite isomerization of the HNS molecule, with subsequent release of NO. Quantum chemistry calculation results are in good agreement with the experimental results. We attribute this laser-induced decomposition as a photo-thermal decomposition for the high temperature rise due to the laser irradiation.

Keywords: 2,2',4,4',6,6'-hexanitrostilbene, photo-thermal decomposition, laser, in-situ XPS, mass spectrometry

1 Introduction

Laser initiation of a high explosive is a complex process and the detonation mechanism occurring during decomposition is not easily identified by chemical physics [1]. Understanding the decomposition mechanisms will allow better control and improvement in the performance of energetic materials for combustion and explosion [2, 3]. The X-ray photoelectron spectroscopic (XPS) technique is an analytical technique for directly observing the surface reaction on the explosive surface, as this technique is highly sensitive to surface characteristics and can provide information on the chemical state and atom ratio in the surface region [4]. XPS studies on the decomposition of energetic materials have been carried out by Sharma *et al.* [5, 6]. They used XPS to study the shock impact, UV irradiation and thermally-induced decomposition of AN, TNT, RDX and TATB. The XPS results provided clear evidence for the cleavage of some specific bonds in the molecules. Xu *et al.* [7] have used the XPS technique to study the decomposition of HMX induced by low energy electron beam irradiation. Their investigations proved that the intensity of the nitro groups of HMX decreased after irradiation compared with those of pristine HMX. The above mentioned studies have provided a good foundation for understanding the shock-, photo-, thermal-, and low energy electron beam irradiation-induced decomposition of energetic materials by using the XPS technique.

In the past, the in-situ XPS technique with prepared, clean and well-characterized surfaces has been widely employed to study the surface region reactions of solid materials. However, the normal XPS spectrum with a poor vacuum environment is easily influenced by the presence of contaminants on the surface, such as water and hydrocarbons [8-13]. Despite there having been extensive in-situ XPS investigations of various solid materials, to our knowledge the study of laser-induced decomposition of energetic materials by in-situ XPS has not yet been achieved. In some studies, the laser-irradiation of solid materials is carried out in air, and the surface is subsequently analyzed using XPS. However, in this procedure, the surface is exposed to the ambient atmosphere during its transfer to the XPS system. Such exposure affects the intrinsic changes from the irradiation since the surface of most solid materials is an active region that may absorb gases and contaminants from the atmosphere [14]. In addition, the XPS technique can only detect the solid products, while the gaseous products produced in the decomposition cannot be detected.

Thus, in the present paper, in-situ X-ray photoelectron spectrometer (XPS) – laser–mass spectrometer on-line equipment is elaborately designed to study the decomposition of solid HNS (see Figure 1) at 532 nm, irradiated by a 10-ns

laser pulse. This "in-situ" arrangement allows the laser-irradiation to be carried out in a vacuum chamber without being exposed to air. The focused laser beam is introduced into the XPS vacuum analyzer chamber vertically through the observation window, and directly irradiates the HNS film. The ultrahigh vacuum (10^{-9} mbar) and extreme cleanliness of the XPS analyzer chamber are fully exploited and the sample can be analyzed using X-rays, without sample displacement, while being irradiated by the laser pulse. In this way, the influence of the ambient atmosphere can be excluded, thus enabling an accurate analysis of the laser-induced surface reaction. In addition, a quadrupole mass spectrometer was installed into the XPS equipment from the observation window of the XPS instrument, so that the gaseous products produced in the decomposition process can also be detected simultaneously.

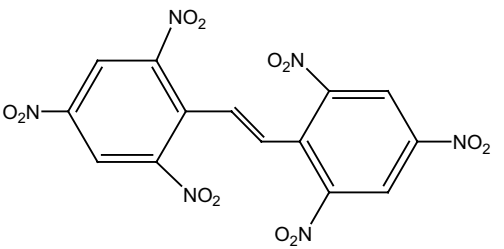

Figure 1. The molecular structure of HNS

2 Experimental

In the experiments, the HNS powder (purity 99.5% determined by HPLC) with an average particle size of 20 μm was pressed to the circular disc, 10 mm in diameter and mounted on double-sided adhesive Scotch tape. XPS apparatus equipped with a laser and a quadrupole mass spectrometer were used for the in-situ XPS system. A schematic illustration of the in-situ XPS – laser – mass spectrometer on-line system is shown in Figure 2. The excitation source was a 10-ns laser beam from an Nd:YAG laser (LS-2131M, LOTIS TII) at a wavelength of 532 nm. The pulse energy of the laser beam was 50 μJ and had a peak intensity $I = 1 \times 10^{12}$ W/cm^2 and fluence $F \approx 1000$ mJ/cm^2, respectively. The laser beam, at a repetition rate of 10 Hz, is initially expanded by a combination of two quartz lenses, one plano-concave lens and another plano-convex lens. The focal lengths of the two lenses were $f_1 = -75$ mm and $f_2 = 400$ mm respectively, and thus the original beam size is magnified 5.3 times to a diameter of 4.8 mm. The laser beam is then focused by a plano-convex lens with a focal length $f_3 = 500$ mm after reflection by

two mirrors M_1 and M_2. The focused laser beam passes vertically through the observation window of the XPS target chamber, leading to an oblique incidence on the sample stage. By carefully measuring the optical path, the focal point of lens L_3 is adjusted to be on the sample stage.

The spatial and temporal distribution of the laser pulse has an almost Gaussian profile. According to the input beam size and the focal length of f_3, the focal spot is calculated as about $D_0 = 70$ μm on the sample surface. In view of the oblique incidence of the laser beam, the actual focal spot size increases to $D'_0 = D_0 / \sin\theta = 109$ μm, where $\theta = 50°$ is the angle between the laser beam and sample stage plane (see Figure 1). Furthermore, energy attenuation by the observation window, which is composed of two layers of glass must be considered. For that purpose, the two glasses were removed for their transmittance measurement. The outer flint glass has a transmittance of $T_1 = 0.85$, while the inner quartz glass has a transmittance of $T_2 = 0.92$ for the 532-nm laser beam. In this way, the transmittance of laser energy from L_3 to the sample surface is $T = T_1/T_2 = 0.78$, which means a 22% attenuation caused by absorption and reflection on the glass window. In the experiments, the pulse energy was 50 μJ and had a peak intensity $I = 1\times10^{12}$ W/cm^2 and fluence $F \approx 1000$ mJ/cm^2, respectively. The XPS spectra and mass spectra were recorded as the laser impinged on the sample. The XPS spectra were obtained with a VG250 X-ray photoelectron spectrometer (VG Scientific, UK) employing Al's Kα-ray for excitation. The instrument was operated at constant analysis energy (CAE) mode with the pressure below 2×10^{-9} mbar. A quadrupole mass spectrometer was installed in the analyzer chamber of the VG250 instrument through the observation window of the XPS instrument to detect the gaseous products from the material during laser irradiation. The quadrupole mass spectra were available in the range 1 to 200 m/z.

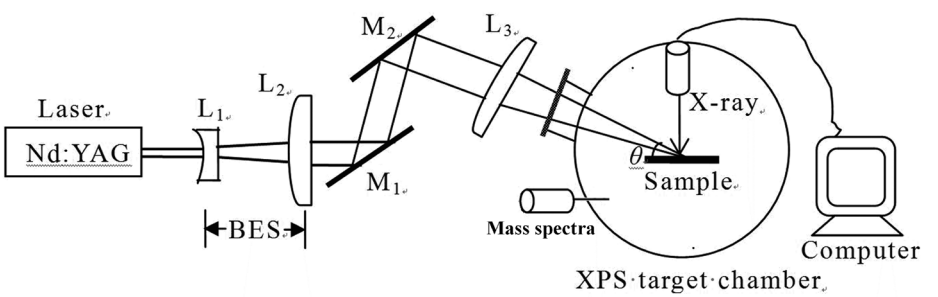

Figure 2. Experimental arrangements for the in-situ XPS of HNS: L_1 – quartz plano-concave lens, L_2-L_3 – quartz plano-convex lens and M_1-M_2 – mirrors

In the quantum chemistry calculations, all molecular structures were optimized by using Density Functional Theory (DFT) at the B3LYP/6-311G (d,p) level. The quantum chemistry calculations were performed by a Gaussian 03 program.

3 Results and Discussions

3.1 XPS characterization

The control XPS spectrum of HNS before irradiation is shown in Figure 3(a). Elemental analysis of the HNS surface by XPS showed only carbon, nitrogen, and oxygen to be present; XPS does not detect hydrogen. The XPS C 1s, N 1s and O 1s narrow scan spectra before laser irradiation are also shown in Figure 3. The C 1s narrow scan spectrum consists of two components, .C*-H and C*-N, which corresponds to binding energies at 284.6 and 287.3 eV, respectively. The N 1s narrow scan spectrum shows only one nitrogen peak located at 405.3 eV, arising from the $–NO_2$ groups on the benzene rings before laser irradiation. The O 1s narrow scan spectrum also shows only one peak at 532.2 eV, which is attributed to the chemical state of O 1s of the NO_2 groups.

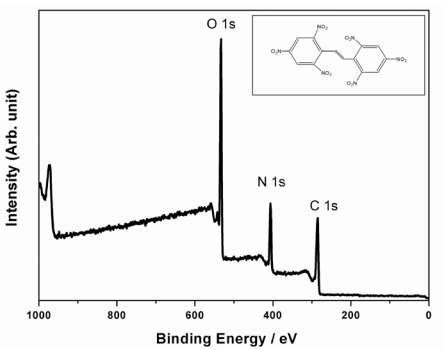

(a)

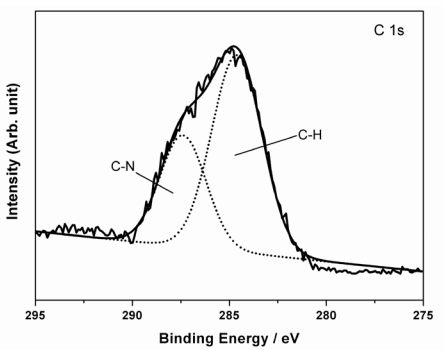

(b)

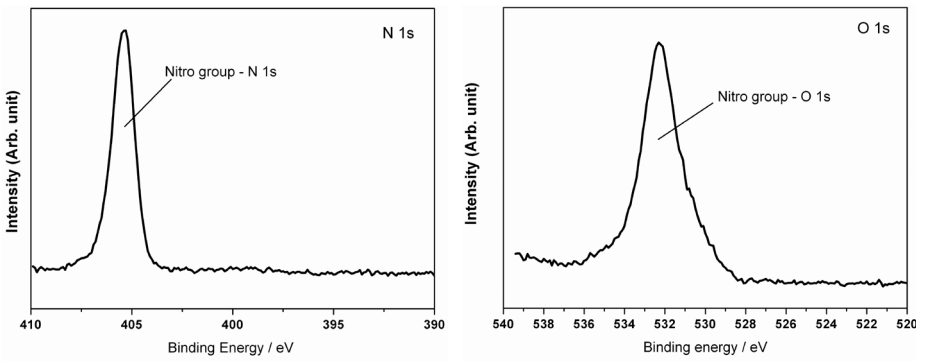

(c) (d)

Figure 3. XPS spectra of HNS before laser irradiation, control spectrum (a), C 1s narrow scan spectrum (b), N 1s narrow scan spectrum (c) and O 1s narrow scan spectrum (d)

Figure 4 shows the time evolution of XPS N1s, O1s and C1s narrow scan spectra of HNS after laser irradiation. For the XPS N 1s spectra, there is only one nitrogen peak located at ~405.5 eV arising from the $–NO_2$ groups on the benzene rings before laser irradiation. After laser irradiation for 5, 10, 15, 20, 30 and 35 min, a new peak at the lower binding energy of 399.7 eV appears, which may be attributed to the chemical state of N 1s of the nitrite ester derivative (–ONO). The intensity of the N 1s peak of the nitrite ester derivative increased slowly as the irradiation time was increased. For the XPS C 1s spectra, spectral changes caused by laser irradiation were also observed. The C 1s spectra are deconvoluted into three Gaussian-type peaks after laser irradiation, while the C 1s spectra are deconvoluted into two Gaussian-type peaks before laser irradiation. The new peak at approximately 288.6 eV is due to the C*–ONO group, which is in agreement with the N1s XPS result. These results indicate that the chemical structure of HNS may be dramatically influenced by the laser irradiation and that nitro-nitrite isomerization occurs in the laser-induced decomposition.

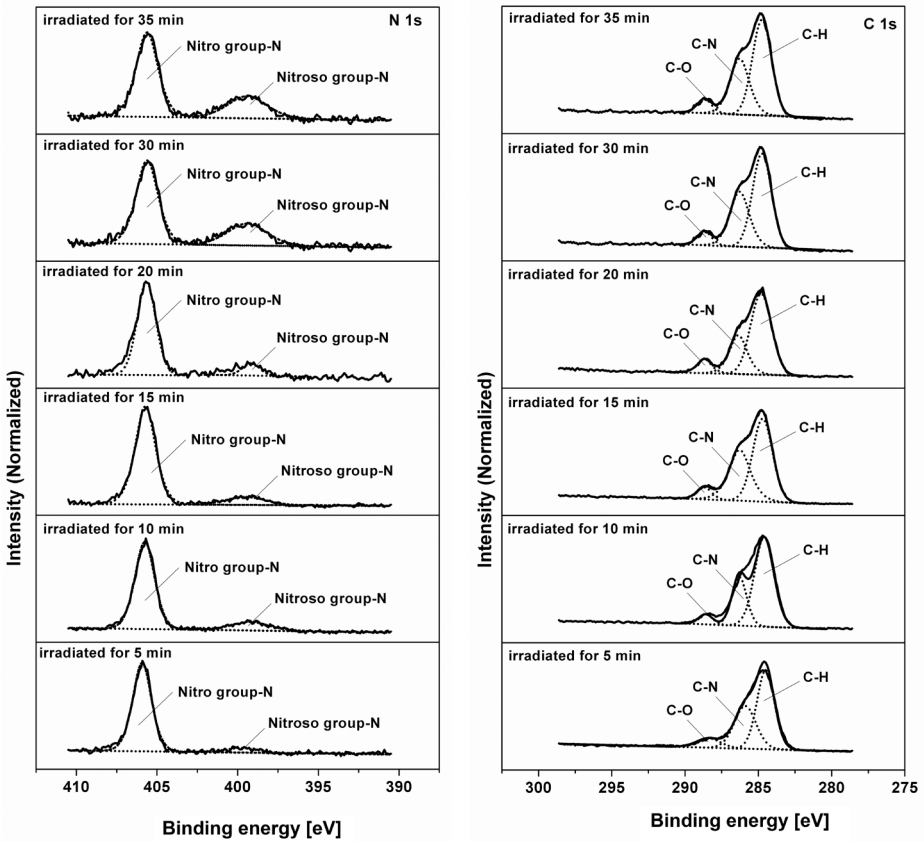

Figure 4. Time evolution of XPS N1s and C1s narrow scan spectra of HNS after laser irradiation

Quantitative evaluation was carried out to further examine the nitro-nitrite isomerization reaction during laser irradiation. A decrease in the [O]/[C] and [N]/[C] ratios and an increase in the [O]/[N] ratio were observed after laser irradiation, as shown in Figure 5, which should not be caused by the nitro-nitrite isomerization reaction alone. One possible explanation is that the nitro-nitrite isomerization reaction occurs with subsequent release of NO in the decomposition.

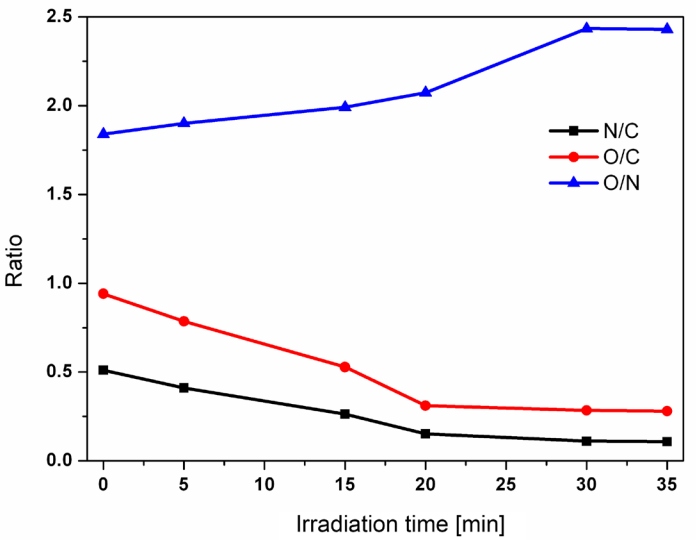

Figure 5. Changes in the [N]/[C], [O]/[C] and [O]/[N] ratios with irradiation time

3.2 Mass spectra

Figure 6 shows the neutral gases desorbing from the HNS sample, with the data obtained using the quadrupole-based residual gas analyser in the ESCALAB analysis chamber. For the residual gas in the XPS target chamber, the gaseous background before laser irradiation was collected first. The gaseous background showed marked peaks at 2, 12, 18, 28, and 44 m/z, which are supposed to come from residual gas in the chamber and attributed to H_2, C, H_2O, N_2/CO and CO_2, respectively. Once the HNS sample is irradiated, the vacuum pressure of the XPS chamber shows a sharp increase (from 2×10^{-9} mbar to 3×10^{-8} mbar) due to the gaseous products produced during the laser induced decomposition. The m/z of the products were distributed in the low molecular weight range (<60 m/z), markedly at 30 amu. Moreover, species at 46 m/z were not detected, which indicates that the nitro groups are transformed to another structure instead of being dissociated from the HNS molecule, while the new peak at 30 m/z is associated with the mechanism of nitro-nitrite isomerization of the HNS molecule with subsequent release of NO. These results further indicate that nitro-nitrite isomerization with subsequent release of NO occurs in the laser-induced decomposition of the HNS molecule.

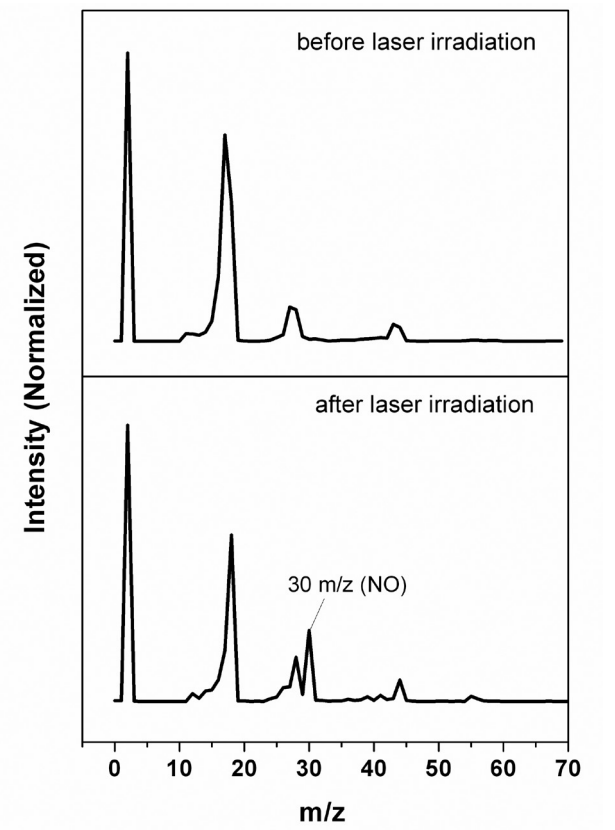

Figure 6. Mass spectra before and after laser irradiation

3.3 Temperature calculation

In these experiments, the energy absorbed from the 532 nm laser results in electronically exciting HNS molecules and can then typically proceed down two different pathways:

(1) the absorbed light energy is converted to internal and translational energy, the excited molecules rapidly undergo internal conversion to the ground state with a high degree of vibrational energy, from which decomposition occurs;
(2) internal conversion or intersystem crossing to another excited state from which the molecule may return to the ground state or couple to a dissociative state resulting in a chemical reaction.

In the first case, the molecule may be in a state that is similar to that resulting from rapid heating, which is called a photothermal decomposition process. In the second case, it may induce a chemical mechanism that is unique and unlike

the thermal pathway, which is called a photochemical decomposition process [15]. Generally, the photothermal and photochemical decomposition mechanisms due to laser initiation compete in the sample and one needs to make a judgment on the basis of the experimental conditions. In the present experiments, long duration laser pulses (10 ns) were used and the photo-induced-thermal effect may become significant. Therefore, an estimate of the temperature for the irradiated sample volume and a comparison with the thermolysis temperature is necessary to determine the decomposition mechanism. To estimate the temperature rise in the solid HNS irradiated by a 10 ns laser pulse, the temperature Equation 1 was numerically integrated versus time t and perpendicular distance x, where ρ, C, and R are the density, heat capacity, and reflectivity of HNS, respectively. $I(t)$ is the irradiance of the laser pulse and k_e is the effective absorption coefficient [16].

$$\frac{\partial T}{\partial t} = \frac{\kappa}{\rho C}\frac{\partial^2 T}{\partial x^2} + \frac{k_e(1-R)I(t)\exp(-k_e x)}{\rho C} \tag{1}$$

Equation 1 was numerically integrated with $T_0 = 293$ K initially to obtain the time dependence of the temperature at different depths within the sample. The values used in the calculation were:

– $\rho = 1.74 \times 10^3$ kg/m^3,
– $C = 1200$ J/(kg·K),
– $k_e = 10^4$ cm^{-1}, (measured in our lab), and
– $R = 0.65$, respectively.

$I(t)$ is represented by a Gaussian pulse of 10-ns (FWHM) width. The calculation assumes that all of the absorbed laser energy is converted to thermal energy. For a peak power density of 10^8 W/cm^2, the calculated temperature curve at a specific depth $x = 50$ nm below the HNS surface is shown in Figure 7. The curves show that the temperature first rises to a maximum within the pulse length and then begins to decay due to thermal conductivity. It can be seen that the temperature rise is higher than the thermolysis temperature of HNS molecules (588 K) due to the effect of the 10 ns laser pulse. The temperature rise may lead to material ablation and a crater on the surface appeared where the laser impinged on the sample; visual inspection showed a dusting of residual black material on the surface. Thus, it is clearly a photo-thermal decomposition mechanism for HNS molecules under these experimental conditions.

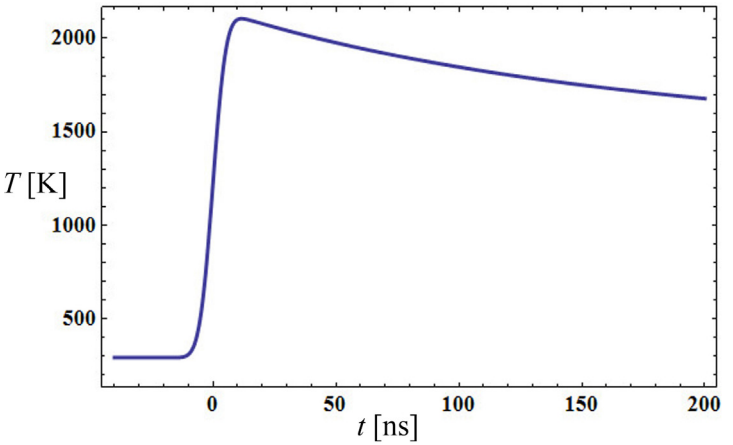

Figure 7. Calculated temperature curve at 50 nm depth below the HNS surface during 532 nm laser irradiation with a 10-ns Gaussian pulse, $F = 1000$ mJ/cm^2

3.4 Quantum chemistry calculations of the HNS molecule

The XPS spectra and mass spectra provide evidence for the nitro-nitrite isomerization with subsequent release of NO in the laser-induced decomposition of HNS. To understand such a chemical transformation of HNS, the structure of HNS was geometry-optimized by B3LYP/6-311G (d, p) in our work. The results suggested that the two benzene rings are not in the same plane. The energy barriers of the decomposition channel of the nitro-nitrite isomerization with subsequent release of NO were also calculated at the level of B3LYP/6-311G(d,p) in Gaussian 03 program, and were 228.03 and –275.02 kJ/mol respectively, as shown in Figure 8. Since this reaction energy barrier is very low theoretically, it is evident that the nitro-nitrite isomerization with subsequent release of NO in the HNS molecule is adopted to occur in the photo-thermal decomposition, which is consistent with the calculation results of some typical energetic materials, such as 1,1-diamino-2,2-dinitroethene [17].

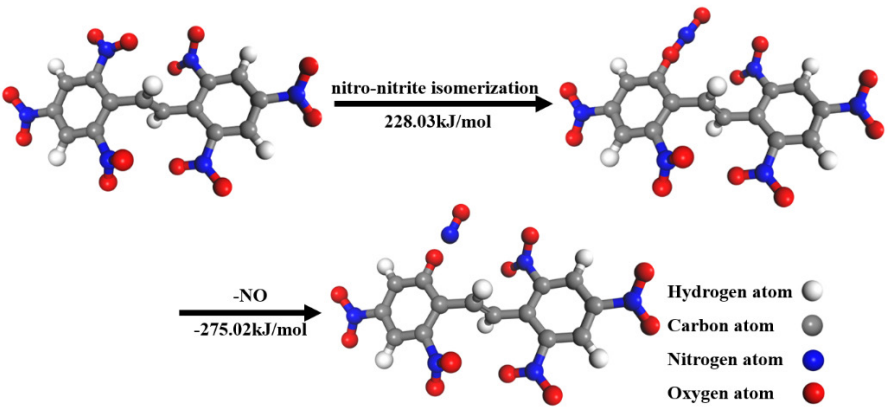

Figure 8. Energy barriers of the decomposition channel of the nitro-nitrite isomerization with subsequent release of NO

It is generally accepted that the nitro groups represent the primary cause of initiation reactivity of polynitro explosives. If the nitro groups transform to another structure, the reaction center might change or lose the reactivity in some cases. Consequently, the properties such as detonation, sensitivity, and safety of the HNS explosive might change after laser irradiation.

4 Conclusions

- In this paper, the laser-induced decomposition of solid HNS has been studied using 10 ns laser pulses at 532 nm by elaborately designed in-situ X-ray photoelectron spectrometer – laser–quadrupole mass spectrometer on-line equipment.
- The new peaks at the binding energy of 399.7 eV of N 1s XPS spectra and of 288.6 eV of C 1s spectra show that nitro-nitrite isomerization with subsequent release of NO occurs in the laser-induced decomposition of HNS. The new peak at 30 m/z in the mass spectrum of the gaseous products further indicates that the nitro-nitrite isomerization occurs with subsequent release of NO in the laser-induced decomposition of the HNS molecule.
- The low energy barrier of the decomposition channel of the nitro-nitrite isomerization with subsequent release of NO calculated by quantum chemistry also proved the feasibility of the mentioned decomposition. A temperature rise calculation showed that a photo-thermal decomposition occurs in these experiments.

Acknowledgments

This work is supported by National Natural Science Fund of China (No. 11802254).

References

[1] Gifers, H.; Pravica, M. Radiation-Induced Decomposition of PETN and TATB. *J. Phys.Chem. A*. **2008***, 112*: 3352.

[2] Im, H.S.; Bernstein, E.R. On the Initial Steps in the Decomposition of Energetic Materials from Excited Electronic States. *J. Chem. Phys.* **2000**, *113*(18): 7911-7918; DOI: 10.1063/1.1315609.

[3] Sun, Y.; Shu, Y.; Xu, T.; Shui, M.; Zhao, Z.; Gu, Y.; Wang, X. Review of the Photodecomposition of Some Important Energetic Materials. *Cent. Eur. J. Energ. Mater.* **2012**, *9*(4): 411-423.

[4] Ohtsu, N.; Masahashi, N.; Mizukoshi, Y.; Wagatsuma, K. Hydrocarbon Decomposition on a Hydrophilic TiO_2 Surface by UV Irradiation: Spectral and Quantitative Analysis Using in-Situ XPS Technique. *Langmuir* **2009**, *25*(19): 11586-11591.

[5] Sharma, J.; Garrett, W.L.; Owens, F.J.; Vogel, V.L. X-ray Photoelectron Study of Electronic Structure and Ultraviolet and Isothermal Decomposition of TATB. *J. Phys. Chem*. **1982**, *86*: 1657.

[6] Owens, F.J.; Sharma, J. X-Ray Photoelectron Spectroscopy and Paramagnetic Resonance Evidence for Shock-induced Intramolecular Bond Breaking in Some Energetic Solids. *J. Appl. Phys.* **1980**, *51*(3): 1494-1497.

[7] Xu, T.; Xiong, Y.; Zhong, F.; Wang, L.; Hao, X.; Wang, H. Chemical Transformation of Octahydro-1,3,5,7-tetranitro-1,3,5,7-tetrazocine (HMX) Induced by Low Energy Electron Beam Irradiation. *Propellants Explos. Pyrotech.* **2011**, *36*(6): 499-504; DOI: 10.1002/prep.201000059.

[8] Serykh, A.I.; Amiridis, M.D. In-Situ X-Ray Photoelectron Spectroscopy Study of Supported Gallium Oxide. *Surf. Sci.* **2010**, *604*: 1002-1005.

[9] Zhang, L.; Takata, K.; Yasui, T.; Tahara, H.; Yoshikawa, T. Effects of Ion Bombardment on Polymer Films. *Mater. Chem. Phys.* **1998**, *54*: 98-101; DOI: 10.1016/S0254-0584(98)00064-9.

[10] Fujii, T.; de Groot, F.M.F.; Sawatzky, G.A. In-Situ XPS Analysis of Various Iron Oxide Films Grown by NO_2-Assisted Molecular-Beam Epitaxy. *Phys. Rev. B* **1999**, *59*(4): 3195-3202.

[11] Zhu, J.F.; Kinne, M.; Fuhrmann, T.; Denecke, R.; Steinrück, H.-P. In-Situ High-Resolution XPS Studies on Adsorption of NO on Pt(111). *Surf. Sci.* **2003**, *529*: 384-396; DOI: 10.1016/S0039-6028(03)00298-X.

[12] Kaichev, V.V.; Miller, A.V.; Prosvirin, I.P.; Bukhtiyarov, V.I. In-Situ XPS and MS Study of Methanol Decomposition and Oxidation on Pd(111) under Millibar Pressure Range. *Surf. Sci.* **2012**, *606*(3-4): 420-425.

[13] Shui, M.; Sun, Y.; Zhao, Z.; Cheng, K.; Xiong, Y.; Wu, Y.; Fan, W.; Yu, J.; Yan, Y.; Yang, Z.; Gu, Y.; Zhong, F.; Xu, T. Photothermal Decomposition of HNS at 532 nm. *Optik* **2013**, *124*(23): 6115-6118; DOI: 10.1016/j.ijleo.2013.04.089.
[14] Ohtsu, N.; Tsuchiya, B.; Oku, M. X-Ray Photoelectron Spectroscopic Study on Initial Oxidation of Hafnium Hydride Fractured in an Ultra-High Vacuum. *Appl. Surf. Sci.* **2007**, 253, 6844.
[15] Glascoe, E.A.; Zaug, J.M.; Armstrong, M.R.; Crowhurst, J.C.; Grant, C.D.; Fried, L.E. Nanosecond Time-Resolved and Steady-State Infrared Studies of Photoinduced Decomposition of TATB at Ambient and Elevated Pressure. *J. Phys. Chem. A* **2009**, *113*: 5881-5887; DOI: 10.1021/jp809418a.
[16] Oldershaw, G.A. Excimer Laser Ablation of Polyethylene Terephthalate. Prediction of Threshold Fluences from Thermolysis Rates. *Chem. Phys. Lett.* **1991**, *186*(1): 23-26; DOI: 10.1016/0009-2614(91)80186-2.
[17] Fu, Q.B.; Shu, Y.J.; Huang, Y.G. Thermal Decomposition Mechanism of FOX-7. (in Chinese) *J. Solid Rocket Technol. (Guti Huojian Jishu)* **2010**, *33*(1): 77-80.

Received: March 08, 2021
Revised: March 30, 2023
First published online: March 31, 2023